Effects of contamination upon the performance of x-ray telescopes

Stephen L. O'Dell[*a], Ronald F. Elsner[a], and Tim Oosterbroek[b]

[a] NASA Marshall Space Flight Center, Space Science Office, MSFC/VP62, Huntsville, AL 35812
[b] ESA European Science Research and Technology Centre, ESTEC/SRE-PAI, PO Box 299, 2200 AG Noordwijk, The Netherlands

ABSTRACT

Particulate and molecular contamination can each impact the performance of x-ray telescope systems. Furthermore, any changes in the level of contamination between on-ground calibration and in-space operation can compromise the validity of the calibration. Thus, it is important to understand the sensitivity of telescope performance---especially the net effective area and the wings of the point spread function---to contamination. Here, we quantify this sensitivity and discuss the flow-down of science requirements to contamination-control requirements. As an example, we apply this methodology to the *International X-ray Observatory* (IXO), currently under joint study by ESA, JAXA, and NASA.

Keywords: X-ray telescopes, molecular contamination, particulate contamination, calibration

1. INTRODUCTION

ESA, JAXA, and NASA are jointly studying the next facility-class x-ray-astronomy mission—the *International X-ray Observatory* (IXO). IXO requires both very large effective area (> 3 m^2 at 1 keV, > 0.6 m^2 at 6 keV) and good angular resolution (< 5″ half-power diameter, HPD), in order to achieve unprecedented sensitivities for the study of the high-redshift Universe and for high-precision spectroscopy of cosmic x-ray sources.

Particulate and molecular contamination can alter the performance of x-ray optical systems[1, 2, 3, 4, 5, 6]—including, of course, the proposed IXO x-ray telescope. In order to optimize the performance of an x-ray telescope and to ensure the stability of its calibration, it is important to understand the sensitivity to contamination and to limit the accumulation of contamination on the x-ray mirrors to a level that does not adversely impact the science goals. Combining the sensitivity analyses with the science requirements leads (Figure 1) to contamination-control requirements, which then drive the contamination-control plan, implementation, and verification.

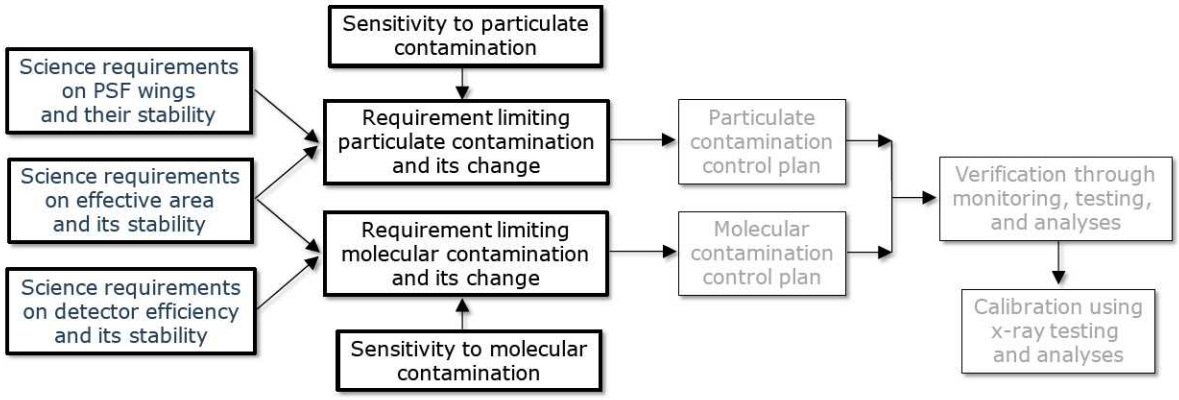

Figure 1: Flow-down of science requirements on a telescope's performance and calibration stability entails analyses of the sensitivity of performance to particulate contamination and to molecular contamination.

[*] Contact author: Steve.O'Dell@nasa.gov; phone +1 256-961-7776; fax +1 256-961-7522; wwwastro.msfc.nasa.gov.

Particulate contamination always degrades x-ray performance (§2) through absorption and diffractive scattering, each of which removes photons from the specular direction. On the other hand, small amounts of molecular contamination, if deposited as a thin film, can improve performance (§3) by increasing the reflectance, at least for some x-ray energies. However, any change in contamination—whether it improves or degrades performance—is problematic, in that it compromises the calibration of the x-ray telescope. We adopt the conservative philosophy that the surest way to limit changes in the level of contamination, is to impose comparable limits on the absolute level of contamination.

Here we review the effects upon the optical performance of grazing-incidence mirrors of particulate contamination (§2) and of molecular contamination (§3), in order to determine the sensitivity of an x-ray telescope's performance to contamination. We next discuss (§4) the results and implications for IXO contamination-control requirements, after which we summarize (§5) our conclusions.

2. PARTICULATE CONTAMINATION

In this section, we first describe (§2.1) the basic effects of particulate contamination upon performance, providing a detailed sketch of the calculations in Appendix A. We then quantify (§2.2) the sensitivity of grazing-incidence telescopes to particulate contamination.

2.1. Basic effects

Particulates—"dust"—decrease the effective area or throughput of an x-ray telescope, through absorption and diffractive scattering of the incident x rays. The diffractively scattered x rays contribute to the point spread function (PSF) of the telescope, at characteristic angles $\vartheta \approx \lambda/(\pi a)$ dependent upon the x-ray wavelength λ and grain radius a. To facilitate this discussion, we treat all particulates as spherical grains: Provided that the particulates are randomly oriented, the precise shape of the grains is not critical in estimating the performance sensitivity and in formulating contamination-control requirements.

The primary parameter quantifying extinction (absorption and scattering) is $F_{\text{Dust}}^{\perp}$, the fraction of the mirror surface projected onto the aperture that is occupied by dust grains. For randomly oriented grains, this projected fractional areal coverage by grains simply scales with fractional areal coverage (viewed normal to the surface) F_{Dust} and inversely with the mirror's grazing angle α:

$$F_{\text{Dust}}^{\perp} = \frac{F_{\text{Dust}}}{\sin\alpha} \ . \tag{1}$$

For a distribution of grain sizes a,

$$F_{\text{Dust}} = \int F_a(a)\,da = \int \left[\pi a^2\right] n_a(a)\,da \ , \tag{2}$$

with $F_a(a)$ the differential fractional areal coverage per grain radius a, equal to the geometric cross-sectional area of the grain times $n_a(a)$, the differential number of grains of radius a per unit surface area.

The expectation values η for absorbing and for scattering a photon of energy E, in a grain on either of the two reflecting surfaces of a (two-reflection) grazing-incidence telescope are, respectively,

$$\eta_{\text{abs}}(E) \approx 2\times 2\times \langle Q_{\text{abs}}(E)\rangle \times F_{\text{Dust}}^{\perp} = 2\times 2\times \langle Q_{\text{abs}}(E)\rangle \times F_{\text{Dust}}/\sin\alpha \ , \tag{3}$$

$$\eta_{\text{scat}}(E) \approx 2\times 2\times \langle Q_{\text{scat}}(E)\rangle \times F_{\text{Dust}}^{\perp} = 2\times 2\times \langle Q_{\text{scat}}(E)\rangle \times F_{\text{Dust}}/\sin\alpha \ . \tag{4}$$

In these equations, one factor of 2 arises because the telescope requires two reflections to reach the focal surface. The other factor of about 2 occurs because a photon may interact with a dust grain either before or after it reflects from a mirror's surface. Consequently, we should consider each grain, not in isolation, but as a grain and its image together. For grazing-incidence mirrors, this nearly doubles the effective cross-section of a grain—thus the second factor of 2. The remaining factor is the grain-size averaged efficiency for absorption or for scattering, respectively:

$$\langle Q_{\rm abs}(E)\rangle \equiv \int Q_{\rm abs}(E,a)\,F_a(a)\,da \,/\, F_{\rm Dust}\ , \tag{5}$$

$$\langle Q_{\rm scat}(E)\rangle \equiv \int Q_{\rm scat}(E,a)\,F_a(a)\,da \,/\, F_{\rm Dust}\ . \tag{6}$$

The expectation value and efficiency for extinction—absorption and scattering combined—are, of course,

$$\eta_{\rm ext}(E) = \eta_{\rm abs}(E) + \eta_{\rm scat}(E)\ , \tag{7}$$

$$Q_{\rm ext}(E,a) = Q_{\rm abs}(E,a) + Q_{\rm scat}(E,a)\ . \tag{8}$$

Given the expectation value η_i for an interaction of type i = abs | scat | ext , the probability of such an interaction is

$$p_i(E) = 1 - \exp\left[-\eta_i(E)\right] \xrightarrow[\eta_i << 1]{} \eta_i\ . \tag{9}$$

Although specific values for the grain-size averaged efficiencies depend upon composition and grain-size distribution, $\langle Q_{\rm ext}(E)\rangle \approx 2$ at soft x-ray energies ($0.1\ {\rm keV} < E < 10\ {\rm keV}$), for reasonable distributions. The balance of absorption and scattering at low energies shifts toward scattering at high energies, as grains become transparent (Appendix A).

Two different diffractive scattering mechanisms can impact the imaging performance of x-ray telescopes: (a) scattering by surface roughness and (b) scattering by particulates. Figure 2 (left panel) compares schematically the point spread function for scattering by surface roughness with that of scattering by particulates. Surface-roughness scattering off a mirror at grazing incidence is highly asymmetric, with the characteristic scattering angle in the plane of reflection exceeding that out-of-plane by a factor $\csc\alpha = 1/\sin\alpha$. In contrast, particulate scattering is quasi-symmetric if the grains are randomly oriented. (Taking into account diffractive scattering of the grain and its image combined, the characteristic in-plane scattering angle would be one-half the out-of-plane one—i.e., $\lambda/(2\pi a)$ versus $\lambda/(\pi a)$.) This pronounced difference in the angular distribution of scattered radiation provides an effective diagnostic for identifying scattering by dust, using intra-focal x-ray images[7] (Figure 2 right panel) or sub-aperture focal images[8] (Figure 3).

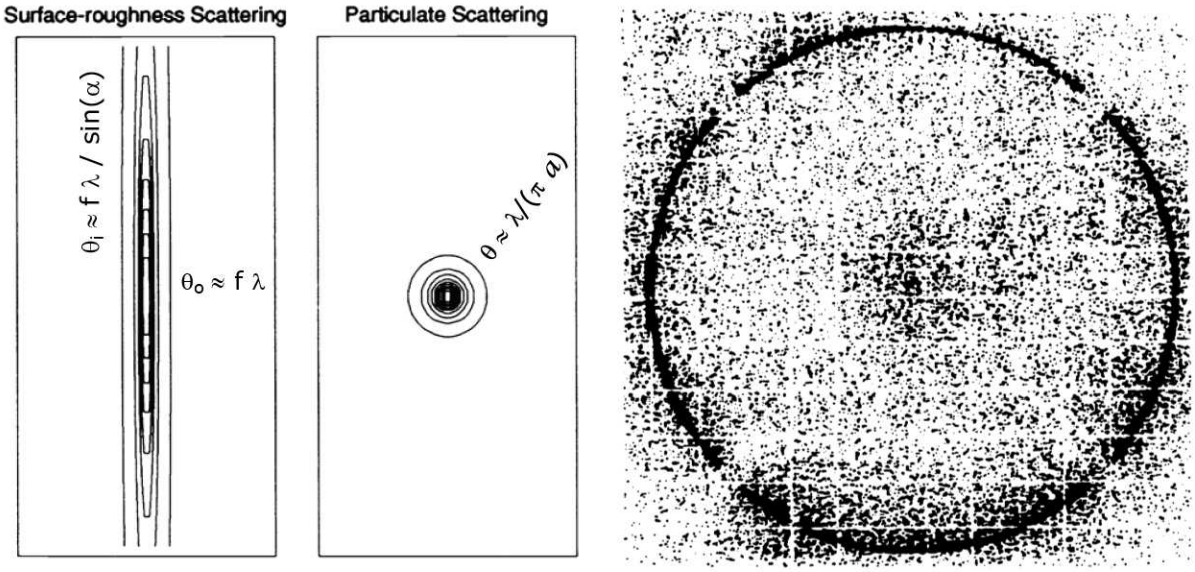

Figure 2: The left panel compares the point spread function for surface-roughness scattering with that for dust scattering. For surface roughness at spatial frequency f , the characteristic scattering angle follows from the grating equation. The right panel displays an intra-focal (1.49-keV) x-ray image obtained during testing VETA-1, the largest Chandra mirror pair prior to final processing and coating with iridium. Scattered x rays partially fill in shadows of radial struts that quadrisect the ring: This out-of-plane scattering indicates that the mirrors were dusty ($F_{\rm Dust} \approx 100\ {\rm ppm}$) at that point. The final Chandra mirror assembly shows little indication of dust scattering (Figure 8). (Diagrams and image are from Reference 7.)

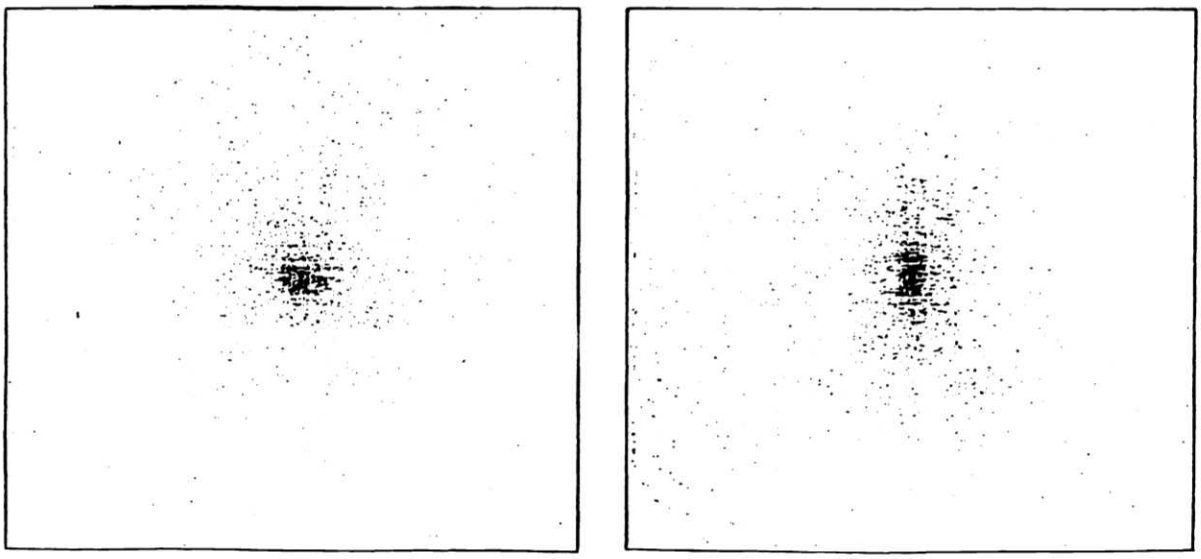

Figure 3: The left panel shows a focused sub-aperture x-ray image at 0.277 keV (C Kα), using the VETA-1 top quadrant; the right panel, at 1.49 keV (Al Kα), using the bottom quadrant. Owing to x-ray energy and location on the mirror, the scattering in the left image is primarily by dust, while that in the right image is primarily by surface roughness. Even in the right image, some scattering is evident in the left and right quadrants, which x rays scattered by surface roughness on the top or bottom quadrants cannot reach. (Images are from Reference 8.)

2.2. Sensitivity

For purposes of formulating compact contamination-control requirements for soft-x-ray telescopes, it usually suffices to limit the fractional change of effective area due to extinction by particulate contamination:

$$\left[\frac{\Delta A_{\rm eff}(E)}{A_{\rm eff}(E)}\right]_{PC} = -\,p_{\rm ext}(E) \xrightarrow[\eta_{\rm ext}<<1]{} -\eta_{\rm ext}(E) \approx -\,2\times 2\times \langle Q_{\rm ext}(E)\rangle \times F_{\rm Dust}^{\perp} \to -2\times 2\times 2\times F_{\rm Dust}/\sin\alpha\ . \qquad (10)$$

Here we use the fact that $Q_{\rm ext} \to 2$ for the energy and grain-size range of interest. Put another way, the grain-size range of interest is that for which $Q_{\rm ext} \approx 2$, which occurs for grains that are thick either to absorption or to dispersion—i.e., when $x^2\left(\beta^2+\delta^2\right) = \left(\beta^2+\delta^2\right)(2\pi a/\lambda)^2 > 1$ (Appendix A). The sensitivity function for particulate contamination is then simply

$$\frac{d\,\ln[A_{\rm eff}(E)]}{d\,F_{\rm Dust}} \cong -\frac{2\times 2\times \langle Q_{\rm ext}(E)\rangle}{\sin\alpha} \to -\frac{8}{\sin\alpha}\ , \qquad (11)$$

which is only weakly dependent upon x-ray E over most of the energy range of interest. In any case, the absolute value of the right-hand side of the above relation serves as a firm upper bound to the magnitude of the sensitivity to particulate contamination at a specified grazing angle α.

3. MOLECULAR CONTAMINATION

In this section, we first describe (§3.1) the basic effects of molecular contamination upon performance, providing a detailed sketch of the calculations in Appendix B. We then quantify (§3.2) the sensitivity grazing-incidence telescopes to molecular contamination.

3.1. Basic effects

Evaluating the effects of molecular contamination upon the performance of x-ray mirrors is more complicated than doing so for those of particulate contamination. The effects of dust are always negative, in that extinction (absorption and scattering) by the particulates always adversely affects performance. In contrast, a thin low-Z (e.g., hydrocarbon) film actually increases the reflectance of a high-Z (e.g., iridium) optical coating at most energies not immediately above the atomic edges of the contaminant[4, 9]. This increased reflectance can be substantial, especially just above the atomic edges of the optical coating.

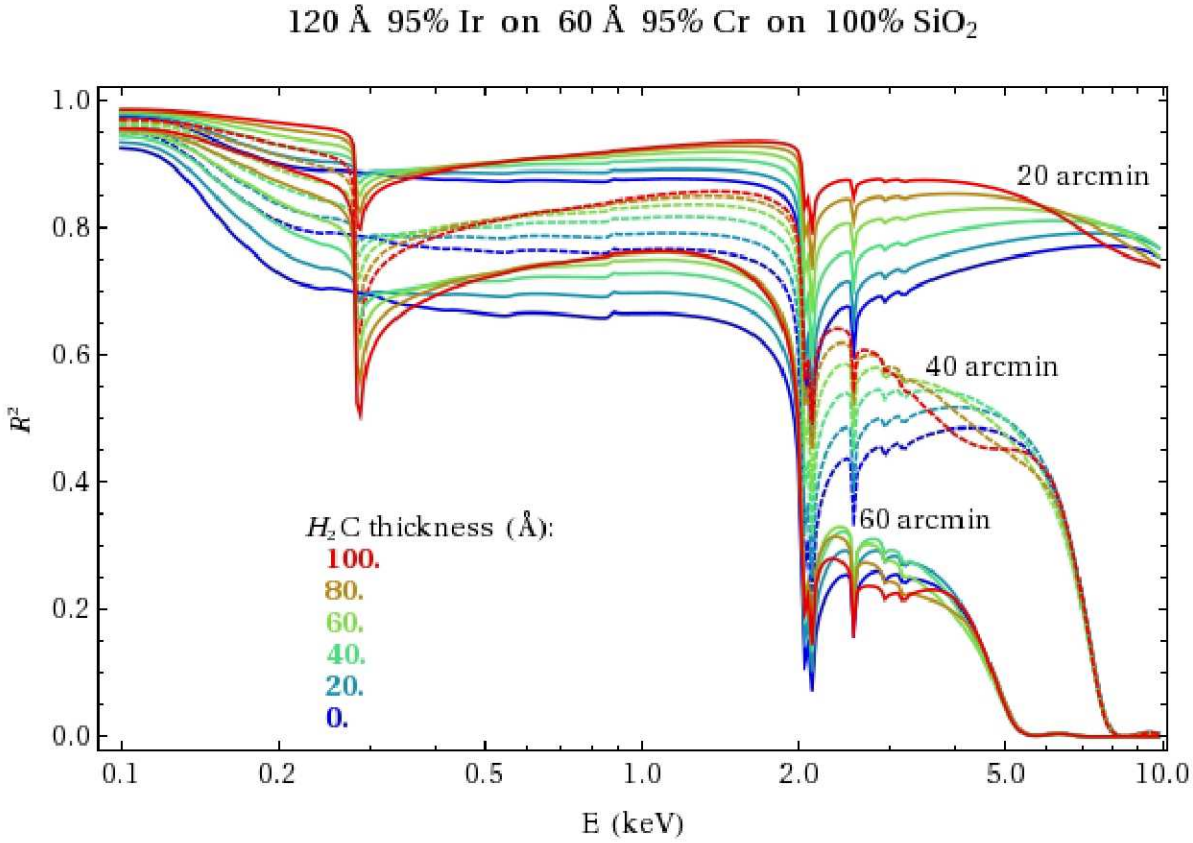

Figure 4: The two-reflection efficiency—i.e., reflectance squared R^2—of a grazing-incidence optic depends sensitively upon the thickness of any molecular film overlaying the optical coating. This figure shows the efficiency for a (bare) iridium optical coating, covered by a hydrocarbon film of unit specific density and thickness 0–100 Å, for 3 grazing angles.

Figure 4 displays the two-reflection efficiency R^2—the square of the reflectance $R(E,\alpha)$ per surface (Appendix B)—for various thicknesses (0–100 Å) of an example molecular contaminant (pure-hydrocarbon film with specific density $\rho = 1$), over an iridium (120 Å at 95% bulk density) optical coating. Less important to the response are the chromium undercoating (60 Å at 95% bulk density) and the silicate substrate. The figure overplots R^2 for three grazing angles (⅓°, ⅔°, and 1°) representative of mirrors covering the soft-x-ray (0.1–10 keV) band. Note that, at most energies not immediately above the carbon K edge (at 0.284 keV), the hydrocarbon film increases the reflectance of the surface. This enhanced efficiency is particularly pronounced just above the iridium M edges (starting at 2.040 keV), but is significant at most energies (away from the carbon edge of the molecular contaminant) below the critical energy (Appendix B) of the optical coating for the mirror's grazing angle α:

$$E_c(\alpha) = \frac{E_p}{\sin\alpha}\sqrt{\frac{f_1}{Z}} = \frac{(0.029\,\text{keV})}{\sin\alpha}\sqrt{\frac{f_1}{A}\rho_{\text{coating}}} \approx \frac{(0.029\,\text{keV})}{\sin\alpha}\sqrt{0.4\,\rho_{\text{coating}}}\ . \qquad (12)$$

Although the effects on performance of a thin molecular film can be positive, stability of the molecular film remains an issue. A change in the film's thickness between on-ground calibration and in-space operation or during operations can compromise the integrity of the calibration—even if the change "improves" performance. Furthermore, substantial molecular contamination can also broaden the PSF of the telescope, through diffractive scattering by the film's microroughness or by condensed droplets. For these reasons, it is important to minimize the accumulation of molecular contaminants.

Overcoating an x-ray mirror's optical coating with a thin layer of a nonvolatile low-Z material (e.g., carbon or boron carbide) can stably alter the reflectance of the mirror[10, 11, 12, 13]. As described above, this thin film enhances the mirror's reflectance at most energies. As we shall see (§3.2), an additional benefit of the low-Z overcoating is that it decreases the sensitivity of the mirror's reflectance to molecular contamination, at least over a significant energy range.

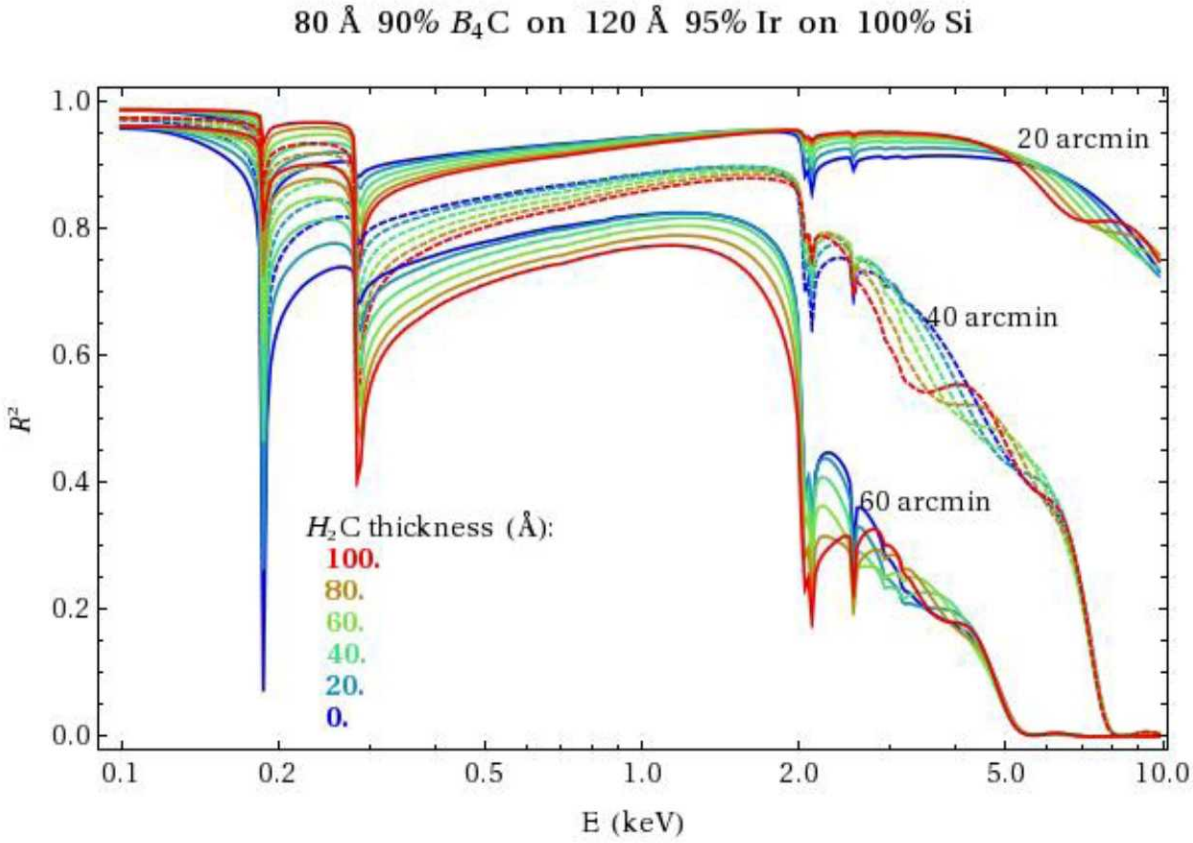

Figure 5: The two-reflection efficiency—i.e., reflectance squared R^2—of a grazing-incidence optic depends sensitively upon the thickness of any molecular film overlaying the optical coating. This figure shows the efficiency for an iridium optical coating with a boron–carbide overcoating, covered by a hydrocarbon film of unit specific density and thickness 0–100 Å, for 3 grazing angles.

Figure 5 bottom panel shows the two-reflection efficiency R^2 for the example hydrocarbon molecular contaminant over an iridium (120 Å at 95% bulk density) optical coating that is overcoated with boron carbide (80 Å at 90% bulk density). Less important to the response is the silicon substrate. The hydrocarbon thicknesses and mirror grazing angles are the same as those in Figure 4. Note that the hydrocarbon film decreases the reflectance at energies between the C K edge and Ir M_V edge, for which it adds to the C K-edge absorption. However, the hydrocarbon film increases the reflectance at most other energies.

3.2. Sensitivity

From the calculations (Appendix B) illustrated by Figure 4 and Figure 5, we can compute the sensitivity of effective area to molecular contamination. The (on-axis) effective area of a (two-reflection) grazing-incidence telescope comprised of S shells is

$$A_{\text{eff}}(E) = \sum_{s=1}^{S} A_{\text{eff},s}(E,\alpha_s) \cong \sum_{s=1}^{S} A_{\text{ap},s}\, R^2(E,\alpha_s) \ , \tag{13}$$

with $A_{\text{ap},s}$ the geometric area of the unobstructed aperture of the s^{th} shell and $R(E,\alpha_s)$ the reflectance at energy E for the mean grazing angle α_s of that shell. Rather than investigate a specific telescope design, which would specify $A_{\text{ap},s}$ and α_s for each shell, we examine the sensitivity to molecular contamination for the two-reflection efficiency at a few grazing angles representative of soft-x-ray telescopes—namely, those used for Figure 4 and Figure 5.

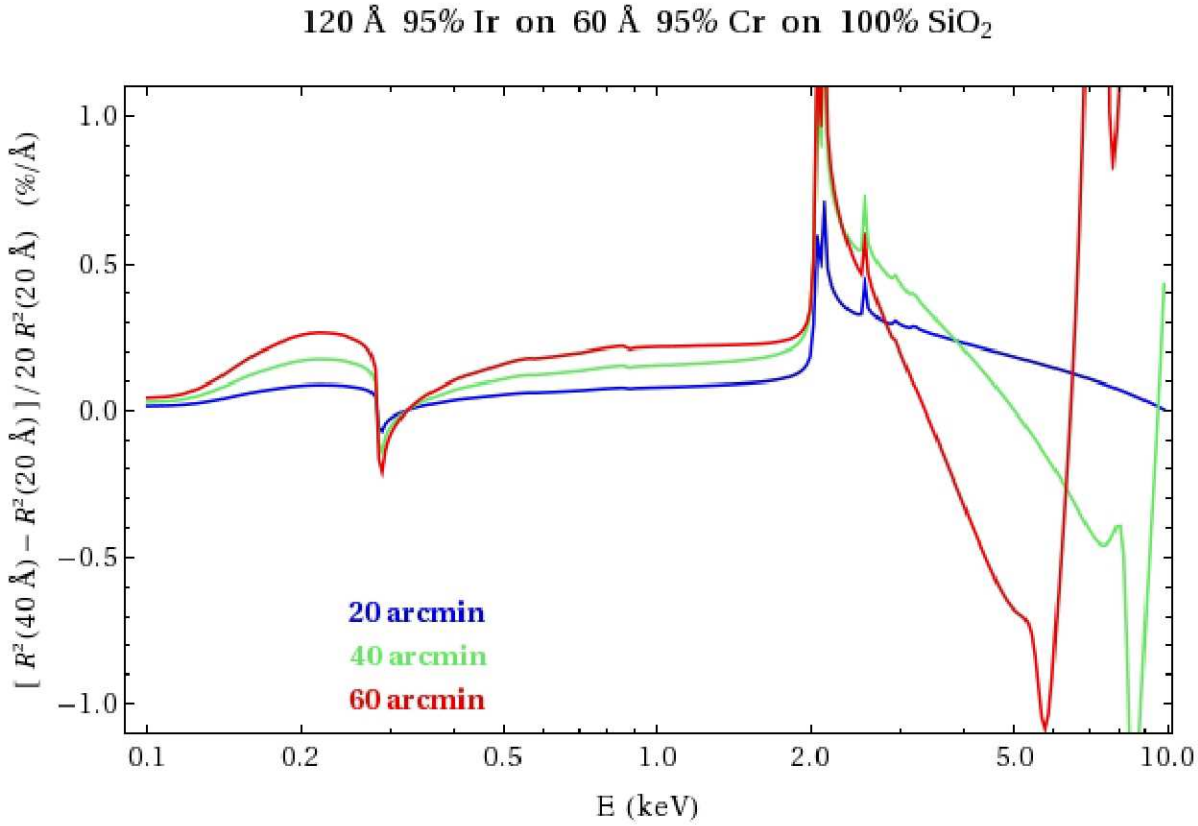

Figure 6: The fractional sensitivity, to molecular contamination, of the two-reflection efficiency of a grazing-incidence optic depends upon the properties of the optical coating and of any overcoating. The sensitivity shown here is in %/Å of a pure hydrocarbon film of unit specific density and nominal 20-Å thickness. This figure shows the sensitivity for a (bare) iridium optical coating, at 3 grazing angles (cf. Figure 4).

In particular, to estimate the sensitivity, we use

$$\frac{d\,\ln\left[A_{\text{eff}}(E)\right]}{d\,\ell_{\text{Film}}} \cong \frac{d\,\ln\left[R^2(E,\alpha;\ell_{\text{Film}})\right]}{d\,\ell_{\text{Film}}} = 2\,\frac{d\,\ln\left[R(E,\alpha;\ell_{\text{Film}})\right]}{d\,\ell_{\text{Film}}} \ , \tag{14}$$

where ℓ_{Film} is the thickness of the contaminating molecular film. In that the fractional change in reflectance is not linear (nor even monotonic) with the film thickness, we need to calculate the above sensitivity over a reasonable range of film thickness: Based upon previous missions, we take this range to be 0–40 Å. However, Figure 4 and Figure 5

suggest that the relationship is fairly linear up to 100 Å at energies for which bilayer interference is not strong. Consequently, we adopt the following sensitivity function:

$$\frac{d\ln\left[A_{\text{eff}}(E)\right]}{d\,\ell_{\text{Film}}} \cong \frac{d\ln\left[R^2(E,\alpha;\ell_{\text{Film}})\right]}{d\,\ell_{\text{Film}}} \to \frac{R^2(E,\alpha;\ell_1+\Delta\ell)-R^2(E,\alpha;\ell_1)}{R^2(E,\alpha;\ell_1)\,\Delta\ell}\ , \tag{15}$$

taking $\ell_1 = 20$ Å and $\Delta\ell = 20$ Å.

Figure 6 shows this sensitivity function for molecular contamination, based upon the calculations leading to Figure 4: a molecular contaminant (pure-hydrocarbon film with specific density $\rho = 1$), on an iridium (120 Å at 95% bulk density) optical coating, over a chromium undercoating (60 Å at 95% bulk density) on a silicate substrate. Figure 7 is for the same molecular contaminant on the coatings used in Figure 5: a boron-carbide (80 Å at 90% bulk density) overcoat over an iridium (120 Å at 95% bulk density) optical coating, on a silicon substrate. As discussed earlier, the sign of the sensitivity changes with energy, as various atomic edges become important. Note that, except at energies just above the boron and carbon K edges (at 0.188 keV and 0.284 keV, respectively), the B_4C overcoating reduces the sensitivity of the reflectance and, hence, two-reflection efficiency to molecular (hydrocarbon) contamination.

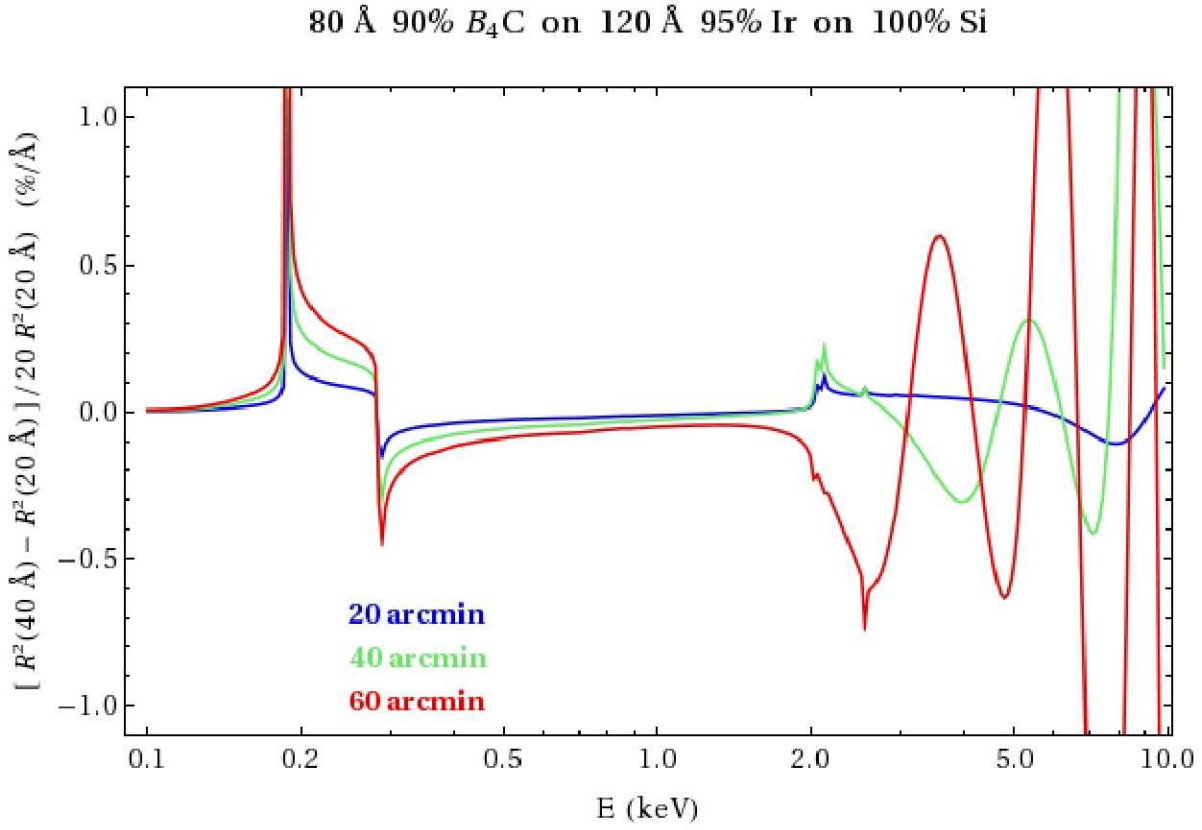

Figure 7: The fractional sensitivity, to molecular contamination, of the two-reflection efficiency of a grazing-incidence optic depends upon the properties of the optical coating and of any overcoating. The sensitivity shown here is in %/Å of a pure hydrocarbon film of unit specific density and nominal 20-Å thickness. This figure shows the sensitivity for an iridium optical coating overcoated with boron carbide, at 3 grazing angles (cf. Figure 5). The large oscillations result from bilayer interference at energies for which the reflectance is generally small.

4. DISCUSSION

Table 1 summarizes the sensitivity of the effective area to particulate contamination (§2) and to molecular contamination (§3), for a range of grazing angles (⅓°–1°) typical of soft-x-ray (0.1–10 keV) telescopes. The sensitivity to particulate contamination is only weakly dependent upon x-ray energy. However, the sensitivity to molecular contamination is strongly dependent upon x-ray energy, due to the importance of the atomic edges of the contaminant, of the optical coating, and of any overcoating.

Table 1: The sensitivity of x-ray-telescope effective area to particulate contamination depends primarily upon grazing angle; that of molecular contamination, upon grazing angle, x-ray energy, and properties of any overcoating.

A_{eff} sensitivity	Particulate	Molecular: CH_2 / Ir			Molecular: CH_2 / B_4C / Ir		
Grazing ∠	F_{Dust}	0.3 keV	1.0 keV	3.0 keV	0.3 keV	1.0 keV	3.0 keV
α = 1°	-0.046%/ppm	-0.07%/Å	+0.22%/Å	+0.18%/Å	-0.25%/Å	-0.05%/Å	-0.17%/Å
α = ⅔°	-0.069%/ppm	-0.05%/Å	+0.15%/Å	+0.42%/Å	-0.17%/Å	-0.03%/Å	-0.05%/Å
α = ⅓°	-0.14%/ppm	-0.02%/Å	+0.08%/Å	+0.29%/Å	-0.08%/Å	-0.01%/Å	+0.06%/Å

Combining science requirements with analyses of the sensitivity of optical performance metrics—effective area, image quality, and their stability—upon particulate and molecular contamination, leads to contamination-control requirements. Here, in order to formulate indicative contamination-control requirements with neither detailed science requirements nor a specific telescope design, we shall require 1% effective-area stability due to changes in particulate contamination and 1%, to changes in molecular contamination. For tighter or more relaxed science requirements, one may scale these indicative contamination-control requirements accordingly. As stated in the Introduction (§1), "We adopt the conservative philosophy that the surest way to limit changes in the level of contamination, is to impose comparable limits on the absolute level of contamination."

Table 2: The contamination-control requirements depend upon the sensitivity of x-ray-telescope effective area to particulate contamination and to molecular contamination, and upon a performance allocation to each. For a 1% stability allocation, this table uses the sensitivities from Table 1 to set limits on the change in level of contamination.

< 1% change	Particulate	Molecular: $\lvert \Delta\ell_{\text{Film}} \rvert$ CH_2 / Ir			Molecular: $\lvert \Delta\ell_{\text{Film}} \rvert$ CH_2 / B_4C / Ir		
Grazing ∠	$\lvert \Delta F_{\text{Dust}} \rvert$	0.3 keV	1.0 keV	3.0 keV	0.3 keV	1.0 keV	3.0 keV
α = 1°	< 22 ppm	< 14 Å	< 5 Å	< 6 Å	< 4 Å	< 19 Å	< 6 Å
α = ⅔°	< 14 ppm	< 21 Å	< 7 Å	< 2 Å	< 6 Å	< 37 Å	< 19 Å
α = ⅓°	< 7 ppm	< 43 Å	< 13 Å	< 3 Å	< 12 Å	< 83 Å	< 18 Å

Based upon Table 2, to achieve 1% stability in the effective area requires controlling the particulate contamination to approximately $\left| \Delta F_{\text{Dust}} \right| < 10$ ppm fractional areal coverage by dust. Requiring 1% stability at all energies—including at relevant atomic edges—would require (Figure 6 and Figure 7) controlling molecular contamination to $\left| \Delta \ell_{\text{Film}} \right| < 1$ Å, less than the thickness of a monolayer: This seems overly demanding of the contamination-control implementation. Consequently, we suggest basing requirements for controlling molecular contamination upon the telescope's broadband response. This response depends upon the energy band used to set the requirement, as well as the choice of optical coating and overcoating.

For example, as Table 1 and comparison of Figure 6 and Figure 7 demonstrate, a boron–carbide overcoating makes the reflectance of overcoated iridium less sensitive than that of bare iridium, to hydrocarbon contamination—excluding energies just above the B and C K edges. Thus, at most energies, an intentional overcoating with a low-Z material not only enhances the reflectance but also reduces the sensitivity to molecular contamination.

Based upon Figure 6, Figure 7, and Table 2, we adopt an indicative compromise requirement—namely, $|\Delta\ell_{\text{Film}}| < 5$ Å, typical of a monolayer—to achieve better than 1% stability effective area over nearly the entire soft-x-ray energy range.

Table 3 summarizes indicative contamination-control requirements for the *International X-ray Observatory* (IXO). For IXO, the table allocates 1% each to effective-area modification due to particulate and to molecular contamination levels at on-ground calibration and to their stability between on-ground calibration and in-space operations: The stated contamination-control requirements scale approximately linearly with the assumed allocation—provided the contamination is not severe. For comparison, Table 3 also shows the contamination-control requirements for the *Chandra X-ray Observatory*[14] and for XMM-*Newton*[15]. The sensitivities for all three telescopes are similar, in that each uses mirrors with comparable grazing angles, in order to cover the soft-x-ray band. Thus the differences in the contamination-control requirements (Table 3) result mainly from differing allocations and choice of energy band for specifying requirements on molecular contamination.

Table 3: Indicative contamination-control requirements for IXO assume (initial) absolute and (subsequent) stability allocations of 1% each for particulate and for molecular contamination. *Chandra*-AXAF and XMM-*Newton* requirements allowed allocations of a couple-to-several percent to each.

Contamination type	**Particulate**		**Molecular**	
Control parameter	$(F_{\text{Dust}})_0$	$\lvert \Delta F_{\text{Dust}} \rvert$	$(\ell_{\text{Film}})_0$	$\lvert \Delta\ell_{\text{Film}} \rvert$
IXO (1% allocations)	< 10 ppm	< 10 ppm	< 5 Å	< 5 Å
Chandra X-ray Observatory	< 26 ppm	< 24 ppm	< 35 Å	< 8 Å
XMM-*Newton*	< 70 ppm	< 70 ppm	< 8 Å	< 7 Å

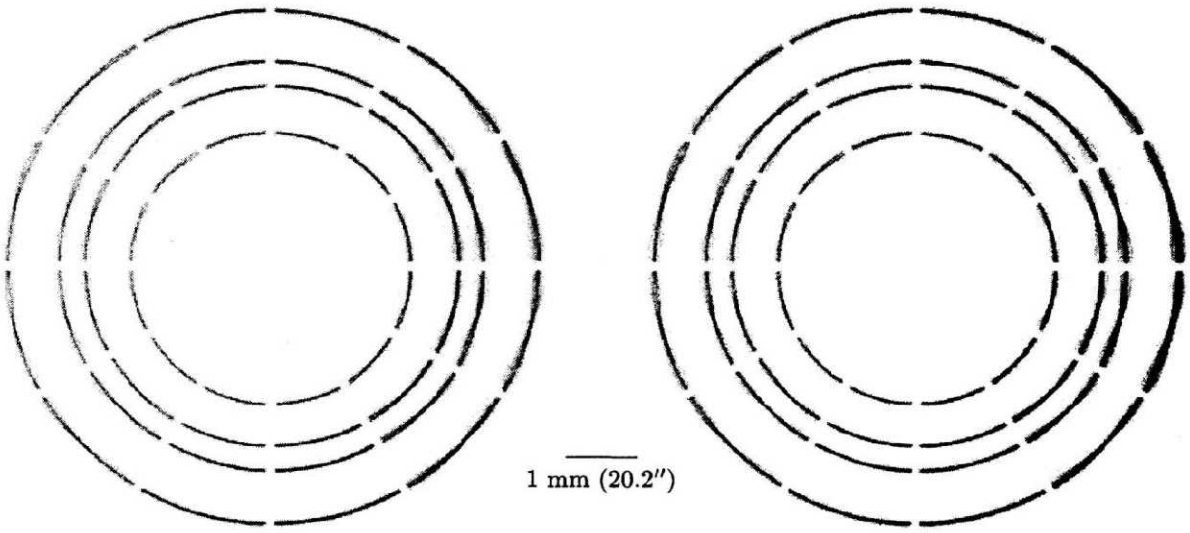

Figure 8: Ring-focus (65-mm intra-focal) images obtained during ground calibration detect essentially no x rays in the shadows of the struts of the *Chandra* (4 mirror-pair) High-Resolution Mirror Assembly (HRMA). The left image is at 0.277-keV (C-Kα); the right, at 1.49-keV (Al-Kα). The pronounced left-to-right gradient is an artifact of the dependence of the quantum efficiency of the microchannel-plate detector upon an x ray's angle of incidence, due to a 6° tilt in the orientation of the top plate's pores. (Images are from Reference 16.)

For the *Chandra X-ray Observatory*, measurements at NASA's X-Ray Calibration Facility (XRCF) and during in-space calibration and science operations have confirmed that the contamination-control requirements are satisfied. There is little evidence for scattering by particulates in images obtained either on the ground or in space. For example, ring-focus

images[16] obtained at the XRCF (Figure 8) show essentially no scattering by dust into the shadows of the telescope's struts (cf. Figure 2 right panel).

Careful re-analyses of spectra obtained during on-ground (XRCF) calibration and in-space operations have measured contamination on the *Chandra* mirrors at a level equivalent to approximately 22 Å of a hydrocarbon film of unit specific density[17, 18]. Comparison of on-ground and in-space data thus far detects no appreciable difference in the level of contamination. In addition, *Chandra* has an on-board Flight Contamination Monitor[19]—a radioactive cadmium (^{109}Cd) source mounted in the HRMA's forward contamination cover—which obtained data at the XRCF and at the start of in-space operations, immediately prior to opening the forward contamination cover. These measurements[20, 21] confirm that any change in the molecular contaminant between on-ground calibration and initial in-space operations was small: Based upon the (electron-capture daughter silver) Ag L-complex lines near 3 keV, the equivalent thickness of the hydrocarbon film changed by $\Delta\ell_{\text{Film}} \approx +3 \pm 1$ Å or, including possible systematic effects, $\left|\Delta\ell_{\text{Film}}\right| < 5$ Å.

Based upon the *Chandra* and XMM-*Newton* experiences, achieving 1% stability in the calibration of the x-ray telescope itself seems achievable. However, limiting the impact of molecular contamination upon the telescope's absolute effective area to 1% may be challenging: A hydrocarbon monolayer could change the effective area by about this amount.

5. SUMMARY

We reviewed and calculated the sensitivities of grazing-incidence telescopes to particulate contamination (§2) and to molecular contamination (§3). Using the computed sensitivities, we suggested contamination-control requirements on the initial level of contamination (at on-ground calibration) and on subsequent changes in the level of contamination, for the *International X-ray Observatory* (IXO). For these indicative requirements, we assumed allocations of 1% (initial) absolute and 1% (subsequent) stability in the effective area, due each to particulate contamination and to molecular contamination. For reference, we compared (§4) these indicative IXO contamination-control requirements with analogous requirements for the x-ray telescope of the *Chandra X-ray Observatory* and those of XMM-*Newton*. In that all these telescopes have similar grazing-angle ranges to span the soft-x-ray band, the sensitivities are comparable.

Although we developed indicative contamination-control requirements on the absolute level of contamination, as well as on the contamination stability, we regard stability to be more important. This is because changes in the level of contamination between on-ground calibration and in-space operation would compromise the utility of the calibration. However, there are diagnostics for estimating the level of contamination or its change, which can be used for in-space calibration, as well as for on-ground calibration. Thus, calibration should be an activity that continues throughout a mission.

Fortunately, contamination-control implementations for *Chandra* and XMM-*Newton* have limited absolute levels of contamination on the x-ray telescopes to acceptable levels. Furthermore, and even more important, the contamination levels on these x-ray telescopes have remained stable over more than a decade from the on-ground calibrations. With appropriate care—including cleanliness during fabrication, isolation of the mirror-assembly cavity whenever possible, and operation at room temperature—telescope effective-area stability at about 1% is achievable.

Unfortunately, previous missions have not been so successful in limiting the accumulation of molecular contamination[22] onto cold surfaces—especially, the filters of cooled detectors. For such detectors, molecular contamination by low-vapor-pressure materials is particularly problematic: Due to their low volatility, these materials outgas slowly, do not effectively vent from the spacecraft, and accumulate onto surfaces too cold for them to vaporize. The most effective approach to ensure that molecular contamination does not become an issue, is to keep all surfaces in the optical path warm. Molecular-migration simulations show[23] that intermittent heating ("bake-out") of filters that normally operate at cryogenic temperatures can aggravate the situation[24, 25], unless the heating thoroughly vaporizes the contaminant from the filter and vents it from the spacecraft or onto a permanently cold surface (cryo-getter). Obviously, the detector should not be the cryo-getter of the observatory.

APPENDIX A

Here we sketch the technical details for calculating the x-ray absorption and diffractive scattering efficiencies—$Q_{\mathrm{abs}}(E,a)$ and $Q_{\mathrm{acat}}(E,a)$, respectively—of a dust grain of radius a. (Because the x-ray refractive index is so close to 1, we can ignore reflection at the grain's surface.) Detailed calculations of these x-ray efficiencies for evaluating particulate contamination generally appear in unpublished reports[26]. However, published investigations[27, 28] of the interaction of cosmic x rays with interstellar grains, document similar calculations. The following summarizes essential equations (e.g., from Reference 28) for calculating efficiencies.

Note that the integrations over cross-section are for an isolated spherical grain; thus, we here ignore interference of the scattering from the grain with that from its image. Generalization to include interference of the grain with its image and other arbitrary grain shapes is conceptually straightforward, albeit mathematically complicated.

We begin with the complex dielectric constant of an elemental material, which we write as

$$\kappa = 1 - \left(\frac{\omega_p}{\omega}\right)^2 \frac{f_1 + i f_2}{Z} = 1 - \left(\frac{E_p}{E}\right)^2 \frac{f_1 + i f_2}{Z}, \tag{16}$$

where $\omega = E/\hbar = 2\pi\nu = 2\pi c/\lambda$ is the angular frequency of the radiation, ω_p and $E_p \equiv \hbar\omega_p$ are the (electron) plasma frequency and the corresponding plasmon energy $E_p \equiv \hbar\omega_p$, and $f_1(E)$ and $f_2(E)$ are respectively the real and imaginary atomic scattering factors[29]. Recall that the plasma frequency (in cgs-Gaussian units) is defined through

$$\omega_p^2 = \frac{4\pi e^2 n_e}{m_e} = \frac{4\pi e^2 \rho}{m_e m_a}\left(\frac{Z}{A}\right), \tag{17}$$

with e the electron's charge, m_e and m_a the electron's mass and the atomic mass unit, ρ the specific density of the material, and Z and A its atomic number and atomic mass. Thus, the plasmon energy is $E_p = (0.029\,\mathrm{keV})\sqrt{\rho\,\mathrm{Z/A}}$.

For a chemical compound of multiple elements indexed by atomic number Z, we approximate the dielectric constant as

$$\kappa \cong 1 - \sum_Z \left(\frac{\omega_p}{\omega}\right)_Z^2 \frac{f_{Z1} + i f_{Z2}}{Z} = 1 - \frac{4\pi e^2 \rho}{m_e m_a} \sum_Z \left(\frac{\rho_Z}{\rho}\right) \frac{f_{Z1} + i f_{Z2}}{A_Z}. \tag{18}$$

Note that the fractional density (ρ_Z/ρ) in element Z is equal to the fractional molecular mass of that element. While this approximation adequately describes the coarse-scale energy dependence of the x-ray dielectric constant of a chemical compound, it does not accurately depict the fine-scale energy dependence: In particular, it does not include the effects of adjacent atoms on the wave function of the photoelectron, which manifest as Extended X-ray Absorption Fine Structure (EXAFS) or X-ray Absorption Near-Edge Structure (XANES) in the absorption coefficient. However, for present purposes, this approximation suffices.

At x-ray energies, the complex refractive index—the square root of the complex dielectric constant κ — is slightly less than unity and can be written as

$$m \equiv 1 - \delta - i\beta \cong 1 - \frac{1}{2}\sum_Z \left(\frac{\omega_p}{\omega}\right)_Z^2 \frac{f_{Z1} + i f_{Z2}}{Z} = 1 - \frac{2\pi e^2 \rho}{m_e m_a} \sum_Z \left(\frac{\rho_Z}{\rho}\right) \frac{f_{Z1} + i f_{Z2}}{A_Z}, \tag{19}$$

where $\delta^2 << 1$ and $\beta^2 << 1$. In this regime, $\delta \approx [1 - \Re(\kappa)]/2$ and $\beta \approx [-\Im(\kappa)]/2$.

The imaginary part $\beta(E)$ of the refractive index and the linear absorption coefficient $\mu_l(E)$ are simply related to through

$$\mu_l(E) = \mu_m(E)\rho = 2\left(\frac{\omega}{c}\right)\beta(E) = \frac{4\pi\,\beta(E)}{\lambda} = \frac{4\pi\,E\,\beta(E)}{hc}\ , \tag{20}$$

with ρ the density of the grain and $\mu_m(E)$ the mass absorption coefficient. Calculating the absorption efficiency of a grain of radius a is conceptually straightforward:

$$\mathrm{Q_{abs}}(E,a) = \int_{b=0}^{a} \{1 - \exp[-\mu_l(E)\,\ell(b)]\}\frac{2\pi\,b\,db}{\pi\,a^2}, \tag{21}$$

where $\ell(b)$ is the path length through the grain as a function of impact parameter b — $\ell(b) = 2\sqrt{a^2 - b^2}$ for $b \le a$.

Calculating the diffractive scattering efficiency is more complicated. The normalized amplitude of the wave in the shadow of the grain, at impact parameter b , is clearly

$$\exp\left[-i\left(\tfrac{2\pi}{\lambda}\right)(m-1)\,\ell(b)\right] = \exp\left[\left(\tfrac{2\pi}{\lambda}\right)(i\delta(E) - \beta(E))\,\ell(b)\right]. \tag{22}$$

Recognizing that the scattered wave amplitude is the above amplitude minus the incident field (Babinet's Principle), Reference 28, for example, uses the Huygens–Fresnel Principle to integrate over the aperture—i.e., grain cross-section—to obtain the diffractive scattering amplitude $S(\vartheta)$ as a function of scattering angle $\vartheta << 1$:

$$\mathrm{S}(\vartheta) = \frac{1}{2\pi}\left(\frac{2\pi}{\lambda}\right)^2 \int_{b=0}^{a} \left\{1 - \exp\left[-i\frac{2\pi}{\lambda}(m-1)\,\ell(b)\right]\right\} J_0\left(\frac{2\pi}{\lambda}\,b\,\vartheta\right) 2\pi\,b\,db\,, \tag{23}$$

with J_0 the Bessel function (of the first kind) of order 0. The differential scattering efficiency is then

$$\frac{dQ_{\mathrm{scat}}(\vartheta)}{d\Omega} = \left(\frac{\lambda}{2\pi}\right)^2 \frac{|\,S(\vartheta)\,|^2}{\pi\,a^2} = \frac{|\,S(\vartheta)\,|^2}{\pi\,x^2}\ , \text{where} \tag{24}$$

$$x \equiv (2\pi\,a/\lambda) = (a\,\omega/c). \tag{25}$$

In order to compute the (integrated) scattering efficiency $Q_{\mathrm{scat}}(E,a)$, one may either integrate the differential scattering efficiency over solid-angle, or simply use

$$Q_{\mathrm{scat}}(E,a) = Q_{\mathrm{ext}}(E,a) - Q_{\mathrm{abs}}(E,a)\ , \tag{26}$$

where the extinction efficiency follows from the real part of the forward scattering amplitude, using the optical theorem:

$$Q_{\mathrm{ext}}(E,a) = 4\pi\left(\frac{\lambda}{2\pi}\right)^2 \frac{\Re[S(0)]}{\pi\,a^2} = 4\pi\,\frac{\Re[S(0)]}{\pi\,x^2}\ . \tag{27}$$

Reference 28 derives analytic expressions for absorption and extinction efficiencies of (isolated) spherical grains. Here we recast these expressions in terms of the refractive-index parameters $\delta(E)$ and $\beta(E)$ and the dimensionless grain-size variable x .

$$Q_{\mathrm{abs}} = 1 - \frac{1}{8\,x^2\beta^2}\left\{1 - e^{-4x\beta}\,[1 + 4x\beta]\right\}; \tag{28}$$

$$Q_{\mathrm{ext}} = 2 - \frac{1}{x^2\left(\beta^2+\delta^2\right)}\left\{\frac{\beta^2-\delta^2}{\beta^2+\delta^2} - e^{-2x\beta}\left[\left(2x\beta + \frac{\beta^2-\delta^2}{\beta^2+\delta^2}\right)\cos(2x\delta) - \left(2x\delta + \frac{2\beta\delta}{\beta^2+\delta^2}\right)\sin(2x\delta)\right]\right\}. \tag{29}$$

Thus the extinction efficiency $Q_{\mathrm{ext}} \to 2$ if the grain is either absorption thick or dispersion thick (large phase change).

APPENDIX B

We compute the reflectance from a multilayer-coated surface over an infinite substrate using a recursive method[30, 31], generalized for arbitrary incidence angle and expressed in notation we employed previously[4, 32]. Here we sketch the technical details of that computation.

Consider an incident wave of wavenumber k_0 entering from vacuum (the 0th layer), at a grazing angle α_0 to the top surface of a stack of J uniform layers, with the last (J^{th}) layer being semi-infinite—i.e., the substrate. Note that we number the layers as $j = 0, 1, \cdots, J$ and the interfaces as $j = 1, \cdots, J$; thus layer j lies between the interfaces j and $j+1$. Given the complex dielectric constant (Appendix A) $\kappa_j = m_j^2$ of the j^{th} layer $(j = 0, 1, \cdots, J)$, the wavenumber k_j in that layer is given by

$$k_j^2 = m_j^2\, k_0^2 = \kappa_j\, k_0^2 = (1 + \Delta\kappa_j)\, k_0^2 \ , \tag{30}$$

where the dielectric increment $(\Delta\kappa_j \equiv \kappa_j - 1)$ is small and negative at x-ray energies and obviously $\Delta\kappa_0 = 0$ for the vacuum. Snell's Law (continuity of k_t) immediately determines the tangential (t) and, with the above equation, normal (z) components of the wavevector in the j^{th} medium:

$$k_{j,t} = k_{0,t} = k_0 \cos\alpha_0 \ ; \tag{31}$$

$$k_{j,z} = \sqrt{k_j^2 - k_{j,t}^2} = k_0\sqrt{\kappa_j - \cos^2\alpha_0} = k_0\sqrt{1 + \Delta\kappa_j - \cos^2\alpha_0} = k_0\sqrt{\sin^2\alpha_0 + \Delta\kappa_j} \ . \tag{32}$$

The (complex) phase change in transiting layer j of thickness $\Delta z_j \equiv (z_{j+1} - z_j)$ is then

$$\Delta\varphi_j = k_{j,z}\, \Delta z_j = k_0\sqrt{\sin^2\alpha_0 + \Delta\kappa_j}\ \Delta z_j \ , \tag{33}$$

for $j = 1, \cdots, J-1$ —i.e., for the layers that are not semi-infinite.

In order to develop a recursive relation for the reflectance of the stacked layers, we first use the electromagnetic boundary conditions to write the Fresnel reflectance amplitudes at the j^{th} boundary, as though layer j were semi-infinite—i.e., ignoring any *reflected* wave in layer j.

$$\left[r_{j-1,j}\right]_{\perp} = \left(\frac{k_{j-1,z} - k_{j,z}}{k_{j-1,z} + k_{j,z}}\right), \tag{34}$$

$$\left[r_{j-1,j}\right]_{\parallel} = \left(\frac{k_j^2\, k_{j-1,z} - k_{j-1}^2\, k_{j,z}}{k_j^2\, k_{j-1,z} - k_{j-1}^2\, k_{j,z}}\right), \tag{35}$$

for linear polarization $\Pi = \perp$ perpendicular and $\Pi = \parallel$ parallel to the plane of incidence.

Next we recursively include the contribution of the reflected wave in layer j to the reflected wave in layer $j-1$. At the last (J^{th}) interface, the full reflectance amplitude, for either polarization Π, is

$$\left[\varepsilon_{J-1}\right]_{\Pi} = \left[r_{J-1,J}\right]_{\Pi} \ , \tag{36}$$

because there is *no* reflected wave in (semi-infinite) layer J —i.e., the substrate. Given the full amplitude of the reflected wave in penultimate layer $J-1$, application of the following recursive relation eventually leads to $\left[\varepsilon_0\right]_{\Pi}$, the amplitude of the reflected wave at the first interface:

$$\left[\varepsilon_{j-1}\right]_{\Pi} = \frac{\left[r_{j-1,j}\right]_{\Pi} + e^{-2i\Delta\varphi_j}\left[\varepsilon_j\right]_{\Pi}}{1 + e^{-2i\Delta\varphi_j}\left[\varepsilon_j\right]_{\Pi}\left[r_{j-1,j}\right]_{\Pi}} \quad . \tag{37}$$

The reflectance at the first interface is then

$$R_{\Pi} = \left|\left[\varepsilon_0\right]_{\Pi}\right|^2 = \left[\varepsilon_0\right]_{\Pi}^{*}\left[\varepsilon_0\right]_{\Pi} \quad . \tag{38}$$

REFERENCES

[1] Hartmann, H., Nord, R., Schwille, H., & Bachor, E., "ROSAT experience on X-ray optics contamination", SPIE 733, 210-216 (1987).

[2] Burkert, W., Aschenbach, B., & Braeuninger, H., "Effects of mirror contamination observed in the ROSAT programme", SPIE 733, 217-227 (1987).

[3] Slane, P., McLaughlin, E. R., Schwartz, D. A., van Speybroeck, L. P., & Bilbro, J. W., "Measurement of the effects of particulate contamination on X-ray reflectivity", SPIE 1113, 12-20 (1989).

[4] Elsner, R. F., O'Dell, S. L., & Weisskopf, M. C., "Molecular contamination and the calibration of AXAF", SPIE 1742, 6-12 (1993).

[5] Kirsch, M. G., Abbey, A., Altieri, B., Baskill, D., Dennerl, K., van Dooren, J., Fauste, J., Freyberg, M. J., Gabriel, C., Haberl, F., Hartmann, H., Hartner, G., Meidinger, N., Metcalfe, L., Olabarri, B., Pollock, A. M., Read, A. M., Rives, S., Sembay, S., Smith, M. J., Stuhlinger, M., & Talavera, A., "Health and cleanliness of the XMM-Newton science payload since launch", SPIE 5898, 0S:1-12 (2005).

[6] Tamura, T., Hara, H., Tsuneta, S., Ichimoto, K., Kumagai, K., Nakagiri, M., Shimizu, T., Sakao, T., & Kano, R., "Contamination evaluation and thermal vacuum bakeout for SOLAR-B visible-light and X-ray telescope", RNAOJ 8, 21-28 (2005).

[7] O'Dell, S. L., Elsner, R. F., Kolodziejeczak, J. J., Weisskopf, M. C., Hughes, J. P. , & Van Speybroeck, L. P., "X - ray evidence for particulate contamination on the AXAF VETA-1 mirrors", SPIE 1742, 171-182 (1993).

[8] Kolodziejczak, J. J., O'Dell, S. L., Elsner, R. F., & Weisskopf, M. C., "Evidence for dust contamination on the VETA-1 mirror surface", SPIE 1742, 162-170 (1993).

[9] Graessle, D. E., Burbine, T. H., Fitch, J. J., Podgorski, W. A., Juda, J. Z., Elsner, R. F., O'Dell, S. L., & Reynolds, J. M., "Molecular contamination study of iridium-coated x-ray mirrors", SPIE 2279, 12-26 (1994).

[10] Pareschi, G., Cotroneo, V., Spiga, D., Vernani, D., Barbera, M., Artale, M. A., Collura, A., Varisco, S., Grisoni, G., Valsecchi, G., & Negri, B., "Astronomical soft x-ray mirrors reflectivity enhancement by multilayer coatings with carbon overcoating", SPIE 5488, 481-491 (2004).

[11] Lumb, D., Christensen, F., Jensen, C., & Krumrey, M., "Influence of a carbon over-coat on the X-ray reflectance of XEUS mirrors", OptCo 279, 101-105 (2007).

[12] Cotroneo, V., Spiga, D., Bruni, R., Burkert, W., Freyberg, M., Hartner, G., Pareschi, G., & Romaine, S., "New developments in light material overcoating for soft x-ray reflectivity enhancement", SPIE 7011, 19:1-10 (2008).

[13] Lumb, D. H., Jensen, C. P., Krumrey, M., Cibik, L., Christensen, F., Collon, M., & Bavdaz, M., "Low atomic number coating for XEUS silicon pore optics", SPIE 7011, 1D:1-10 (2008).

[14] Ryan, L. E., "Contamination control and implementation plan", TRW document AXAF SE28 (1995).

[15] Kirsch, M. G., Abbey, A., Altieri, B., Baskill, D., Dennerl, K., van Dooren, J., Fauste, J., Freyberg, M. J., Gabriel, C., Haberl, F., Hartmann, H., Hartner, G., Meidinger, N., Metcalfe, L., Olabarri, B., Pollock, A. M., Read, A. M., Rives, S., Sembay, S., Smith, M. J., Stuhlinger, M., & Talavera, A., "Health and cleanliness of the XMM-Newton science payload since launch", SPIE 5898, 0S:1-12 (2005).

[16] Zhao, P., Cohen, L. M., & Van Speybroeck, L. P., "AXAF HRMA mirror ring-focus measurements", SPIE 3113, 106-123 (1997).

[17] Chandra X-ray Center, "High-Resolution Mirror Assembly (HRMA)", [*Chandra* Proposers' Observatory Guide, Rev. 12.0, TD 403.00.012], http://cxc.harvard.edu/proposer/POG/, Chapter 4, 33-60 (2009).

[18] Gaetz, T. J., Edgar, R. J., Jerius, D. Wargelin, B., & Zhao, P., "*Chandra* HRMA effective area", [IACHEC 2010], http://web.mit.edu/iachec/meetings/2010/Presentations/Gaetz_hrma.pdf, 1-18 (2010).

[19] Elsner, R. F., Joy, M. K., O'Dell, S. L., Ramsey, B. D., & Weisskopf, M. C., "Ground-to-orbit transfer of the AXAF-I flux scale: in-situ contamination monitoring of x-ray telescopes", SPIE 2279, 332-342 (1994).

[20] Elsner, R. F., O'Dell, S. L., Ramsey, B. D., Tennant, A. F., Weisskopf, M. C., Kolodziejczak, J. J., Swartz, D. A., Engelhaupt, D. E., Garmire, G. P., Nousek, J. A., Bautz, M. W., Gaetz, T. J., & Zhao, P., "Calibration results for the AXAF flight contamination monitor", SPIE 3444, 177-188 (1998).

[21] Elsner, R. F., Kolodziejczak, J. J., O'Dell, S. L., Swartz, D. A., Tennant, A. F., & Weisskopf, M. C., "Measurements with the Chandra X-ray Observatory's flight contamination monitor", SPIE 4012, 612-618 (2000).

[22] IACHEC Contamination Working Group, "Report of Contamination Working Group", [IACHEC 2010], http://web.mit.edu/iachec/meetings/2010/Presentations/ContaminationWG.pdf, 1-11 (2010).

[23] O'Dell, S. L., Swartz, D. A., Plucinsky, P. P., Freeman, M. A., Markevitch, M. L., Vikhlinin, A. A., Chen, K. C., Giordano, R. J., Knollenberg, P. J., Morris, P. A., Tran, H., Tice, N. W., & Anderson, S. K., "Modeling contamination migration on the Chandra X-ray Observatory", SPIE 5898, 313-324 (2005).

[24] Plucinsky, P. P., O'Dell, S. L., Tice, N. W., Swartz, D. A., Bautz, M. W., DePasquale, J. M., Edgar, R. J., Garmire, G. P., Giordano, R., Grant, C. E., Knollenberg, P., Kissel, S., LaMarr, B., Logan, R., Mach, M., Marshall, H. L., McKendrick, L., Prigozhin, G. Y., Schwartz, D., Schulz, N. S., Shropshire, D., Trinh, T., Vikhlinin, A. A., & Virani, S. N., "An evaluation of a bake-out of the ACIS instrument on the Chandra X-Ray Observatory", SPIE 5488, 251-263 (2004).

[25] Urayama, F., Bando, T., Kano, R., Hara, H., Narukage, N., & Sakao, T., "Molecular Contamination Assessments on <i>Hinode</i> X-Ray Telescope", JSASS 56, 536-542 (2008).

[26] Van Speybroeck, L. P., "Dust", Smithsonian Astrophysical Observatory memorandum, March 27 (1987).

[27] Van de Hulst, H. C., [Light Scattering by Small Particles], John Wiley & Sons, New York (1957).

[28] Martin, P. G., "On the interaction of cosmic x rays with interstellar grains", MNRAS 149, 221-235 (1970).

[29] Henke, B. L., Gullikson, E. M., & Davis, J. C., "X-Ray Interactions: Photoabsorption, Scattering, Transmission, and Reflection at E = 50-30,000 eV, Z = 1-92", ADNDT 54, 181-342 (1993).

[30] Morales, J. J., & Nuevo, M. J., "A general method for calculating reflection and transmission coefficients in multiple slabs", AmJPh 59, 1140-1143 (1991).

[31] Lecaruyer, P., Maillart, E., Canva, M., & Rolland, J., "Generalization of the Rouard method to an absorbing thin-film stack and application to surface plasmon resonance", ApOpt 45, 8419-8423 (2006).

[32] Elsner, R. F., O'Dell, S. L., & Weisskopf, M. C., "Effective area of the AXAF X-ray telescope: Dependence upon dielectric constants of coating materials", JXST 3, 35-44 (1991).

Effects of contamination upon the performance of x-ray telescopes

Stephen L. O'Dell[1], Ronald F. Elsner[1], & Tim Oosterbroek[2]

[1] NASA Marshall Space Flight Center (MSFC), Huntsville, AL 35812 (USA)

[2] ESA European Space Research & Technology Centre (ESTEC), 2200 AG Noordwijk (Netherlands)

ABSTRACT

Particulate and molecular contamination can each impact the performance of x-ray telescope systems. Furthermore, any changes in the level of contamination between on-ground calibration and in-space operation can compromise the validity of the calibration. Thus, it is important to understand the sensitivity of telescope performance—especially the net effective area and the wings of the point spread function—to contamination. Here, we quantify this sensitivity and discuss the flow-down of science requirements to contamination-control requirements. As an example, we apply this methodology to the *International X-ray Observatory* (IXO), currently under joint study by ESA, JAXA, and NASA.

Introduction

ESA, JAXA, and NASA are jointly studying the next facility-class x-ray-astronomy mission—the *International X-ray Observatory* (IXO). IXO requires both very large effective area (>3 m^2 at 1 keV, >0.6 m^2 at 6 keV) and good angular resolution (<5″ half-power diameter, HPD) in order to achieve unprecedented sensitivities for the study of the high-redshift Universe and for high-precision spectroscopy of cosmic x-ray sources.

Particulate and molecular contamination can alter the performance of x-ray optical systems. In order to optimize the performance of an x-ray telescope and to ensure the stability of its calibration, it is important to understand the sensitivity to contamination and to limit the accumulation of contamination on the x-ray mirrors to a level that does not adversely impact the science goals.

Particulate contamination of x-ray mirrors

Particulates—i.e., dust—decrease the effective area or throughput of an x-ray telescope, through absorption and diffractive scattering of the incident x rays. The diffractively scattered x rays contribute to the point spread function (PSF) of the telescope, at characteristic angles $\vartheta_{\rm scat} \approx \lambda/(\pi a)$ dependent upon the x-ray wavelength λ and grain radius a.

The expected number ν of grain interactions per x ray is proportional to $F_{\rm Dust}$ (fractional areal coverage by dust of the mirror surface) divided by the projection factor $\sin\alpha$ (ratio of aperture area to surface area for a grazing-incidence mirror). Two factors of 2 arise because an x ray may interact with a dust grain either before or after each reflection and on either the primary or secondary mirror.

Molecular contamination of x-ray mirrors

Evaluation of the effects of molecular contamination upon the performance of x-ray mirrors is more complicated. A thin low-Z (e.g., hydrocarbon) film actually increases the reflectance of a high-Z (e.g., iridium) optical coating at most energies away from the atomic edges of the contaminant. This increased reflectance can be substantial, especially just above the atomic edges of the optical coating.

Although the effects on performance of a thin molecular film can be positive, the stability of the molecular film remains an issue. A change in the film's thickness between ground calibration and in-space operation or during operation can compromise the integrity of the calibration—even if the change "improves" performance. Furthermore, substantial molecular contamination can also broaden the PSF of the telescope, through diffractive scattering by the film's microroughness or by condensed droplets. For these reasons, it is important to minimize the accumulation of a molecular contaminant.

Overcoatings

Overcoating an x-ray mirror's optical coating with a thin layer of a nonvolatile low-Z material (e.g., carbon or boron carbide) can stably alter the reflectance of the mirror. As described above, this thin film enhances the mirror's reflectance at most energies. An additional benefit of the low-Z overcoating is that it decreases the sensitivity of the mirror's reflectance to molecular contamination, at least over a significant energy range.

Conclusions

Combining science requirements with analyses of the sensitivity of optical performance metrics—effective area, image quality, and their stability—upon particulate and molecular contamination, leads to contamination-control requirements. For a range of grazing angles (½°–1°, say) typical of soft-x-ray (0.1–10 keV) telescopes, 1% stability of the effective-area calibration would set the following approximate requirements on contamination control:

- Change in fractional areal coverage by particulates, $|\Delta F_{\rm Dust}| < 2\times10^{-5}$;
- Molecular-film change, $|\Delta\ell| < 4$ Å (on Ir), 20 Å (on B_4C/Ir) for 1 keV. Stability will be worse just above relevant atomic edges.

The safest philosophy for preventing large changes in contamination levels is to limit the absolute levels of contamination.

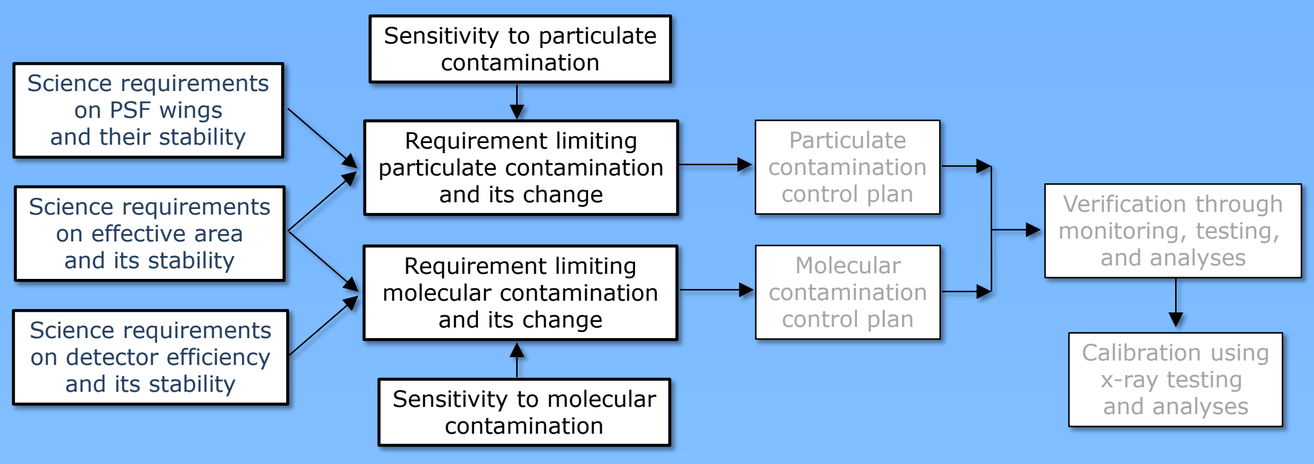

Science requirements and sensitivity studies lead to contamination-control requirements. These requirements drive the contamination-control plan, implementation, and verification.

$$F_{\rm Dust}^{\perp} = F_{\rm Dust}/\sin\alpha\,; \quad F_{\rm Dust} = \int F_a(a)\,da = \int \left[\pi a^2\right] n_a(a)\,da\,;$$

$$\nu_{\rm abs}(E) \approx 2\times2\times\langle Q_{\rm abs}(E)\rangle\times F_{\rm Dust}/\sin\alpha\,, \quad \langle Q_{\rm abs}(E)\rangle \equiv \int Q_{\rm abs}(E,a)\,F_a(a)\,da\,/\,F_{\rm Dust}\,;$$

$$\nu_{\rm scat}(E) \approx 2\times2\times\langle Q_{\rm scat}(E)\rangle\times F_{\rm Dust}/\sin\alpha\,, \quad \langle Q_{\rm scat}(E)\rangle \equiv \int Q_{\rm scat}(E,a)\,F_a(a)\,da\,/\,F_{\rm Dust}\,;$$

$$\nu_{\rm ext}(E) = \nu_{\rm abs}(E) + \nu_{\rm scat}(E), \quad Q_{\rm ext}(E,a) = Q_{\rm abs}(E,a) + Q_{\rm scat}(E,a).$$

$F_{\rm Dust}$ is the fractional areal coverage of a mirror's surface by particulates; $F_{\rm Dust}^{\perp}$, the fractional areal coverage projected onto the aperture. $F_a(a)$ is the fractional areal coverage per grain radius a; $n_a(a)$, the number of grains per unit surface area per grain radius a. $\langle Q_{\rm abs}(E)\rangle$, $\langle Q_{\rm scat}(E)\rangle$, and $\langle Q_{\rm ext}(E)\rangle$ are grain-size-averaged absorption, scattering, and (total) extinction efficiencies, respectively. While specific values for these efficiencies depend upon composition and grain size distribution, $\langle Q_{\rm ext}(E)\rangle \approx 2$ at x-ray energies of interest for reasonable size distributions.

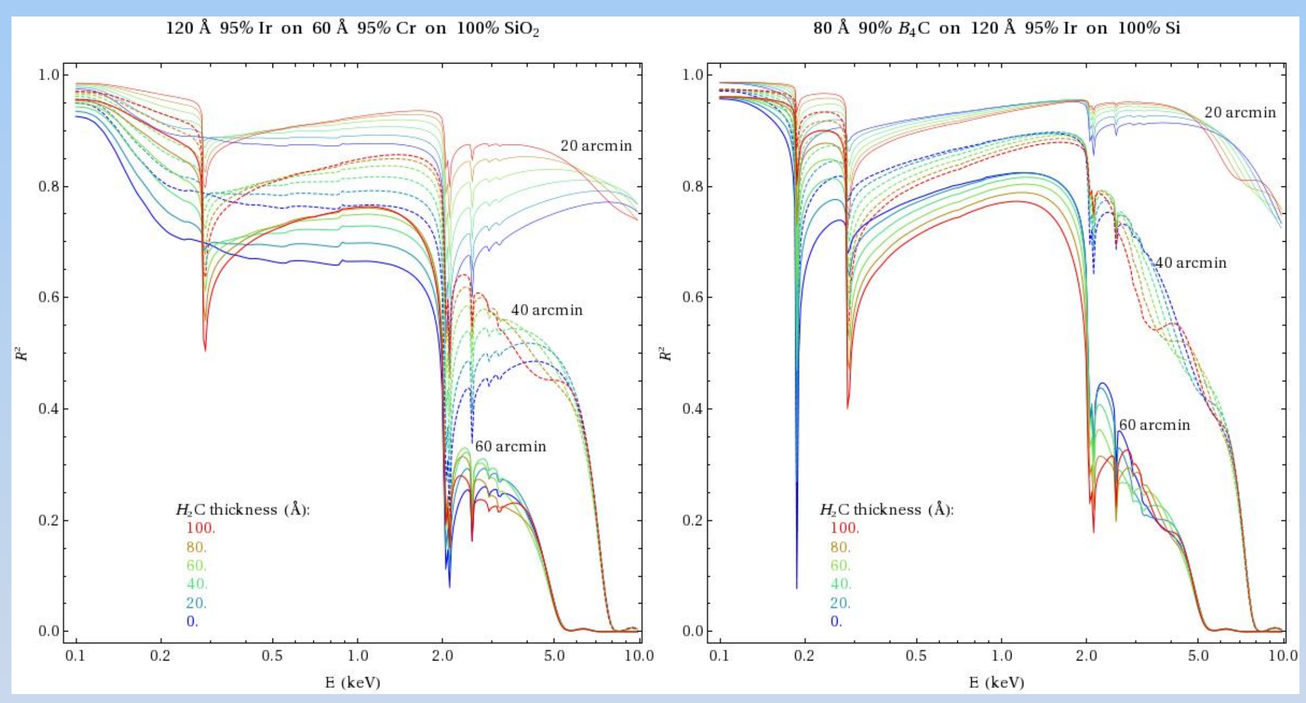

Dependence of two-reflection efficiency—i.e., squared reflectance—upon thickness of a (pure hydrocarbon, specific density ≈1) molecular film on an iridium optical coating, without (left) and with (right) a boron-carbide overcoating, for three grazing angles: 20′, 40′, and 60′.

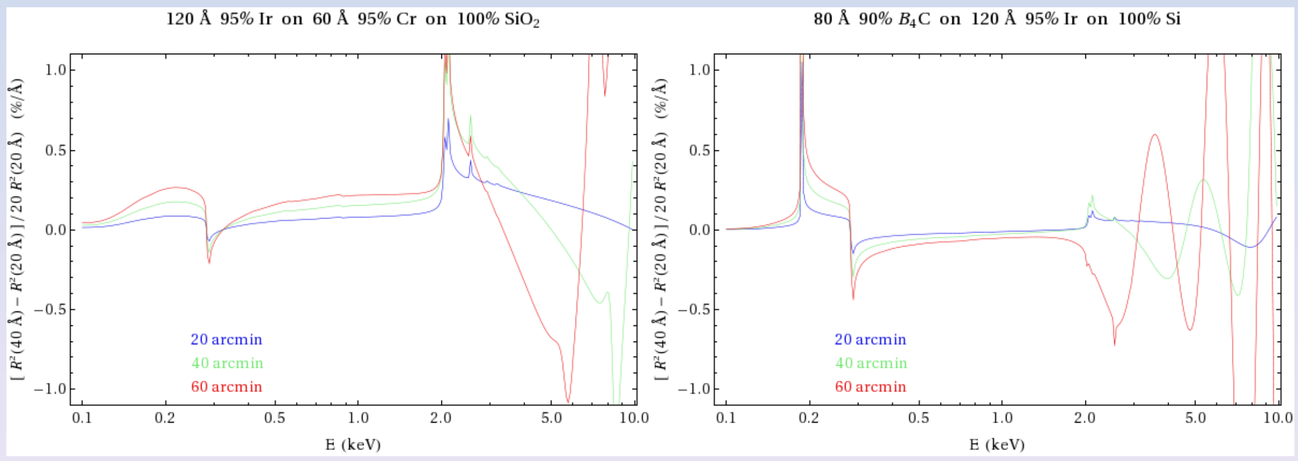

Sensitivity of the two-reflection efficiency upon change in molecular-contaminant thickness, for a nominal 20-Å hydrocarbon film. Sensitivity is for 3 grazing angles: 20′, 40′, and 60′.

Sensitivity	Particulate	Molecular: CH_2 / Ir			Molecular: CH_2 / B_4C / Ir		
Grazing ∠	$F_{\rm Dust}=10^{-5}$	0.3 keV	1.0 keV	3.0 keV	0.3 keV	1.0 keV	3.0 keV
α = 60′	-0.46%	-0.07%/Å	+0.22%/Å	+0.18%/Å	-0.25%/Å	-0.05%/Å	-0.17%/Å
α = 40′	-0.69%	-0.05%/Å	+0.15%/Å	+0.42%/Å	-0.17%/Å	-0.03%/Å	-0.05%/Å
α = 20′	-1.38%	-0.02%/Å	+0.08%/Å	+0.29%/Å	-0.08%/Å	-0.01%/Å	+0.06%/Å